Electrochimica Acta 487 (2024) 144197

Contents lists available at ScienceDirect

Electrochimica Acta

journal homepage: www.journals.elsevier.com/electrochimica-acta

Exploring the reactivity of $Na_3V_2(PO_4)_3$/C and hard carbon electrodes in sodium-ion batteries at various charge states

Ijaz Ul Mohsin [a,*], Andreas Hofmann [b], Carlos Ziebert [a]

[a] Institute of Applied Materials – Applied Materials Physics (IAM-AWP), Karlsruhe Institute of Technology, Karlsruhe, Germany, Hermann-von-Helmholtz-Platz 1, Eggenstein-Leopoldshafen 76344, Germany
[b] Institute for Applied Materials – Materials Science and Engineering (IAM-WK), Karlsruhe Institute of Technology, Karlsruhe, Germany

ARTICLE INFO

Keywords:
Sodium battery
Calorimetry
Thermal stability
States of charge
Evolved gases

ABSTRACT

The interest in post-lithium batteries as an alternative to lithium-ion batteries boosted recently due to their substantial abundance, low cost, inherent safety, and sustainability. In recent years, the crucial need for the improvement of battery safety has been emphasized and safety remains a critical barrier for post-lithium technology. Therefore, the thermal stability and reaction enthalpies of electrochemically de-sodiated sodium vanadium phosphate ($Na_3V_2(PO4)_3$/C) positive electrode and commercial coconut-shell derived hard carbon (HC) at various states of charge (SOCs) were systematically investigated. This study employed the 3D Tian-Calvet calorimeter (C80) and thermogravimetric analysis coupled with mass spectrometry (TGA-MS), to gain comprehensive insights into the thermodynamic aspects of these materials. Thermal stability of electrode materials at distinct sodiation / de-sodiation states draws great attention in cell design and is one of the reasons for the strong state of charge (SOC) dependence of the thermal runaway phenomenon, which represents the most critical safety issue for batteries. This combined experimental approach provides a comprehensive understanding of thermal stability and associated reactions in both, sodium vanadium phosphate (NVP) and hard carbon (HC) electrodes. NVP/C reacts with the electrolyte between 150 and 300 °C, releasing ~400 J/g heat, although it thermally decomposed beyond 150 °C. The sodiated HC initiates decomposition at 100 °C, releasing ~750 J/g heat in two steps in a reaction to the electrolyte. These data can facilitate optimizing the design of thermal management systems according to the cell's thermal performance.

1. Introduction

The thermal stability of cathode materials poses a significant challenge when battery size is upscaled for energy storage applications. Sodium-ion batteries raise safety concerns compared to lithium-ion batteries, mainly attributed to the lower melting point of pure sodium and its higher reactivity compared to lithium [1]. Various studies [2–8] have focused on assessing the thermophysical properties of lithium-based cathode materials at varying temperatures, commonly encountered in the production of lithium-ion batteries. Lim et al. [9]. and Jin et al. [10]. have explored the thermal stability of sodium-based cathode material (NASICON) alongside electrochemical performance. Zhao et al. [11]. delved into investigating the thermal properties of the α-$NaFeO_2$ cathode for Na-ion batteries, employing a combination of liquid electrolytes. They demonstrated the reaction kinetics with varying amounts of liquid electrolyte. Recently, Kobayashi et al. [12]. determined the temperature-dependent lattice constants, thermal expansion, and z-coordinates of P2- and O3-type Na_xMO_2 cathode material. Furthermore, Bak et al. [13]. conducted a study on the thermal stability of charged

$Na_{1-x}MO_2$ cathode materials, enabling the simultaneous observation of structural changes and evolved gas species, especially O_2, during the thermal decomposition of charged cathode materials. Thermal cycling and oxidation behaviour of the nanostructured ceramic has also been studied [14,15]. Despite these advancements, a detailed thermal characterization and a study of the reactivity with binder at different states of charge of sodium cathode/anode materials remains an area of active interest.

The thermal stability of de-lithiated lithium-layered oxide materials has been thoroughly examined through a variety of techniques, among which thermogravimetric Analysis (TGA) combined with mass spectroscopy and differential scanning calorimetry (DSC) are prominent

* Corresponding author.
E-mail address: ijaz.mohsin@kit.edu (I.U. Mohsin).

https://doi.org/10.1016/j.electacta.2024.144197
Received 1 February 2024; Received in revised form 11 March 2024; Accepted 30 March 2024
Available online 30 March 2024

[16–18]. In these studies, the Li-NMC compounds exhibit significantly higher onset temperatures and reduced heat release during the exothermic reaction compared to the Li/Mn-rich compounds after activation. A higher manganese content appears to have adverse effects on both, high-rate performance and thermal stability. The structural evolution of silicon anode during lithiation and de-lithiation is systematically examined through isothermal calorimetric methods [19]. The enthalpy of crystallization of $Li_{15}Si_4$ is quantified, and the parasitic effects, such as the heat of side reactions in pure silicon, are reported. The anode, especially a carbon-based anode, poses a potential hazard for sodium batteries due to the free energy of combustion associated with carbon as reported in lithium batteries [20]. Therefore, the safety of sodium batteries relies also on the intricate interactions among all the cell components especially the sodiated anode e.g., HC.

In this study, our emphasis is to investigate the interactions among cathode/anode materials at different states of charge with the electrolyte and binder system. The thermal behaviour of the materials, both with and without electrolyte (1 M $NaClO_4$ in EC:DMC:EMC = 1:1:1 + 2 wt.% FEC), was examined using 3D Tian Calvet calorimetry (C80) and thermogravimetric analysis coupled with mass spectroscopy (TGA-MS). Furthermore, the reactions involving NVP/C and HC with the electrolyte were extensively explored through sealed-container experiments and respective enthalpies were calculated. The obtained results reveal a notable state-of-charge-dependent potential for reactions between NVP/C and the electrolyte, as well as between HC and the electrolyte. The analysis focuses on understanding how $Na_3V_2(PO_4)_3$/C and hard carbon electrodes respond to different charge states, with a particular emphasis on thermal behaviour. The findings will contribute to a comprehensive understanding of the electrochemical and thermal aspects of these electrodes, aiding in the development of safer and more efficient sodium-ion battery technologies.

2. Experimental procedure

The anode material for electrochemical tests was prepared by combining active material (HC, Kuraray kuranode), styrene butadiene rubber/carboxymethyl cellulose (SBR (BM-4xx (Zeon) /CMC (MAC500LC (Nippon Paper)), and carbon black (TIMCAL C-NERGY Super C65 (Imersy)) at a weight ratio of 93:5.6:1.4 using water as a solvent and details about binder materials manufacturers and process can be found in [21,22]. For the cathode materials, a mixture of self-synthesized active materials (NVP/C) containing 9.8 % carbon [23], PAA/SBR/CMC, and carbon black was prepared at a weight ratio of 92:6:2 in water solvent. The summarized information is presented in Table 1.

Both slurries were cast on an aluminum foil current collector and then dried and calendared. The electrodes, with 10–11 mg cm^{-2} (cathode), 5–6 mg cm^{-2} (anode) loading of active materials, were assembled in 2032-type coin cells (MTI Corp. USA) in an Ar-filled glovebox. The commercial electrolyte was 1 M $NaClO_4$ in a 1:1:1 vol ratio of ethylene carbonate (EC), dimethyl carbonate (DMC), and ethyl methyl carbonate EMC plus 2 vol.% fluoroethylene carbonate (FEC). The formation procedure of the sodium-ion cells for calorimetry and thermal studies consisted of three full charge-discharge cycles using the calculated capacity and a BioLogic cycler (Germany). Then each cell was charged and discharged at 25 °C using their measured capacity. After the formation of cells, different states of charge of $Na_3V_2(PO4)_3$/C and HC were obtained by electrochemical de-sodiation/sodiation from 2.3 to 3.9 V and from 2.0 to 0 V, respectively, at C/10 current rate. Afterwards, the coin cells with different states of charge adjusted were carefully disassembled inside an Ar-filled glovebox. Then, immediately respective electrodes were thoroughly rinsed in dimethyl carbonate (DMC) solvent for thermal studies without electrolyte. Subsequently, all rinsed electrodes were dried at 60 °C for 24 h under a vacuum of 10^{-3} bar inside the Ar-filled glovebox. The electrodes were studied including the current collector (aluminum foil) with the purpose of not changing the electrode system drastically. The harvested electrodes were analysed at six distinct states of charge i.e., 0 %, 20 %, 40 %, 60 %, 80 %, and 100 %. The thermal stabilities and gas evolution of the samples were examined by thermogravimetric analysis (TGA) coupled with mass spectrometry (MS) (Netzsch Jupiter 449 F3). Samples were loaded in an alumina crucible and heated at the rate of 5 K min^{-1} under an argon flow of 50 ml min^{-1}. The dried samples were carefully sealed inside a small container within the glovebox before being transported to the TGA.

For the 3D calorimetric experiments, the pristine electrodes were tested with and without electrolyte. The charged electrodes were tested along with the electrolyte right after the cells were disassembled. The electrodes were directly sealed in the small cylindrical container without washing inside the glovebox. The samples were analysed in a 3D Tian-Calvet (Setaram Instruments) using a temperature scan rate of 0.5 K min^{-1} from 25 °C to 300 °C. The heat flow signal was measured for the entire sample (mass of electrodes plus mass of electrolyte, subtracting the mass of current collector (aluminum foil)) for both positive (NVP/C) and negative (HC) electrodes. The measured enthalpies were normalized by the total weight of the solid sample (without aluminum foil) as well as considering the mass of the liquid electrolyte.

Table 1
Electrodes slurry formulation.

Recipe	Contents (wt. %)	Recipe	Contents (wt. %)
NVP/C	92.03	HC	93
Polyacrylic acid (PAA)	2.3	Carbon black	1.40
Carbon black	2.0	CMC	1.87
Carboxymethyl cellulose (CMC)	0.92	SBR	3.73
Styrene butadiene rubber (SBR)	2.75		

3. Results and discussion

To elucidate the electrochemical characteristics of the electrode materials, half-cells in coin-cell configuration of respective materials were assembled and formatted by three complete cycles. Fig. 1 depicts the standard voltage profiles of NVP/C (theoretical capacity 117 $mAhg^{-1}$) versus sodium (Fig. 1a) and HC (theoretical capacity 350 $mAhg^{-1}$) versus Na (Fig. 1b), along with the corresponding galvanostatically measured capacities of respective coin-cells and coulombic efficiencies (CE). The measured capacity of NVP/C (15 mm diameter disc) is 2.1 mAh (activable capacity of ~104 $mAhg^{-1}$) and of HC is 2.6 mAh (activable capacity of ~265 $mAhg^{-1}$) after irreversible capacity loss of around 14 %.

Before proceeding into the examination of coated electrodes, the thermal stability of pristine electrode materials (as received) and the binder system (as received) employed in the slurry fabrication process were investigated under argon atmosphere. Fig. 2 presents the thermogravimetric analysis (TGA-MS) data for NVP/C powder (as received) and HC powder (as received), while Fig. 3 illustrates the thermal characteristics of the individual binder components. In the case of NVP/C material (Fig. 2a), a distinct H2O peak is evident at 100 °C, corresponding to absorbed water or moisture. Subsequently, a second mass loss begins at an onset temperature of 800 °C, indicative of the thermal decomposition of the compound (NVP/C), leading to the evolution of CO molecules through the carbon reaction with the oxygen present in the compound. Notably, NVP/C exhibits a remarkable thermal stability up to 800 °C under argon atmosphere.

For HC (Fig. 2b), the initial mass loss is attributed to the release of water/moisture, represented by a sharp H_2O peak observed between 100 −150 °C. Subsequently, slower mass loss above 400 °C is probably related to partial decomposition of carbonaceous residues [24], resulting in the evolution of CO/CO_2 molecules through the carbon reaction

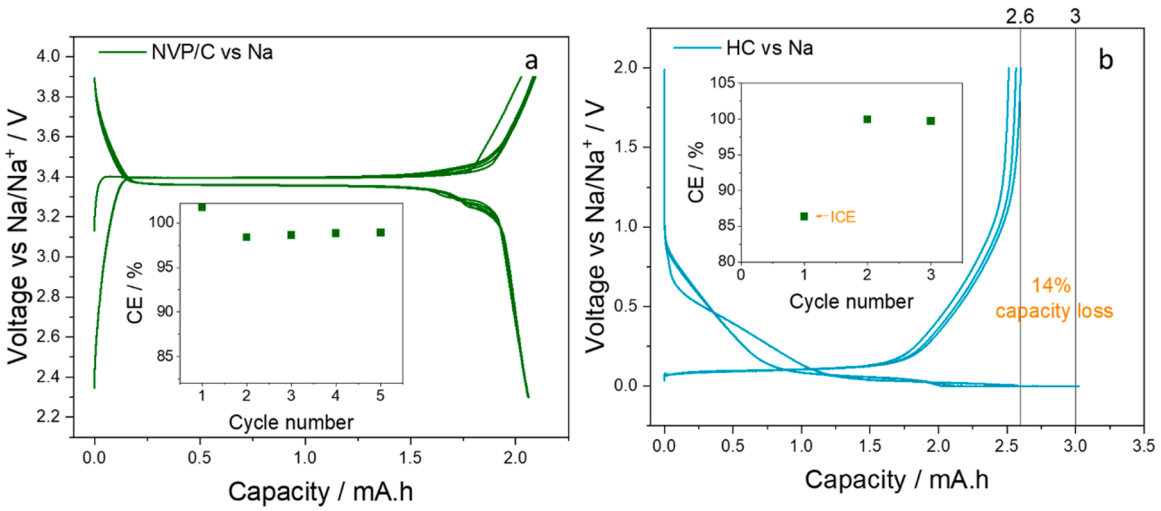

Fig. 1. Operating voltage profiles of NVP/C and HC vs. Na/Na^{+} corresponding electrodes vs. measured capacities. The accompanying Coulombic Efficiency (CE) is shown in the insets.

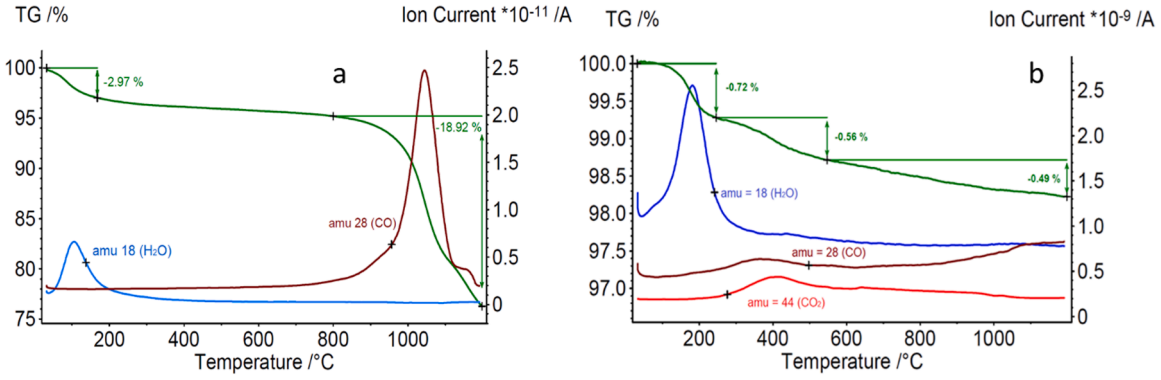

Fig. 2. Thermal stability of (a) pristine NVP/C powder material and (b) HC powder material under argon atmosphere.

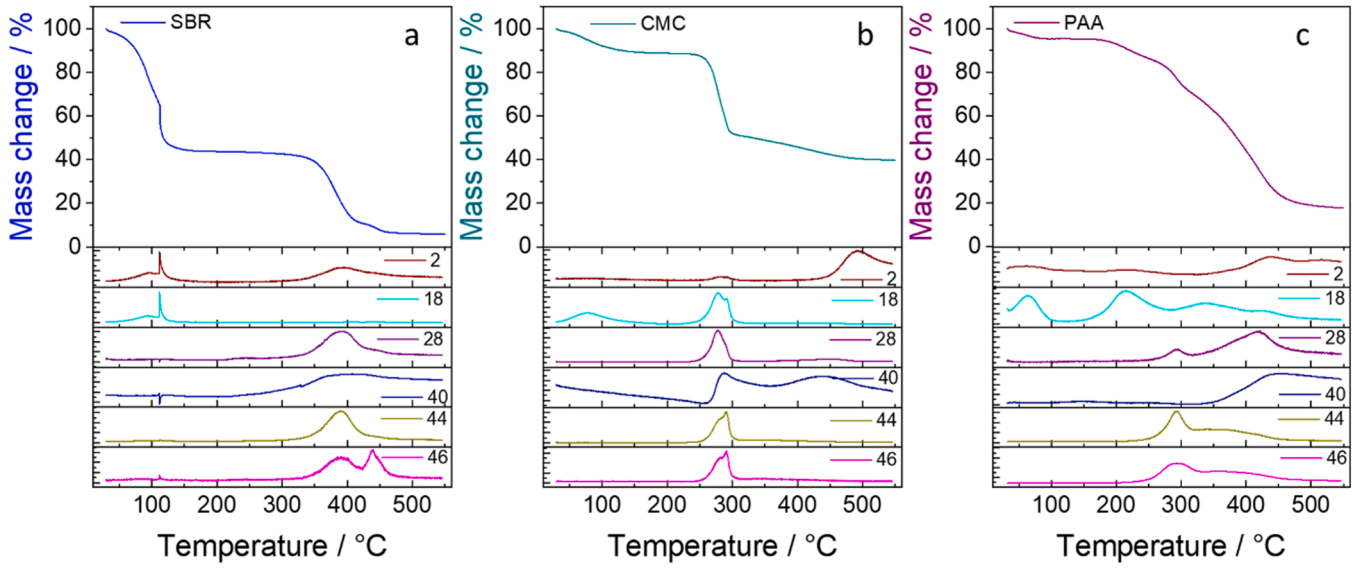

Fig. 3. Thermal stability of binder components are shown: (a) water-suspension of styrene butadiene rubber (SBR), (b) carboxymethyl cellulose (CMC), (c) poly-acrylic acid (PAA) under argon atmosphere.

with the H_2O present in the compound.

The abrupt mass reduction observed at 100 °C in SBR (Fig. 3a) is attributed to a significant water loss. SBR is initially in a suspension form in a water solvent, exhibiting thermal stability up to 350 °C. Beyond this temperature, the release of hydrocarbon gases occurs. Conversely, the CMC demonstrates an initial minor water loss at 100 °C, followed by decomposition at 250 °C, resulting in a substantial 60 % mass loss extending up to 550 °C (Fig. 3b). Similarly, PAA (Fig. 3c) exhibits comparable thermal mass losses, with an 80 % reduction observed up to 550 °C. The evolved gases are summarised in Table 2.

Moreover, when electrode materials are blended with binder components and coated onto an aluminium sheet, it signifies the occurrence of reactions between the electrode materials and the binder components. In the TGA data (Fig. 4a), a pronounced weight loss is observed between 300 °C – 350 °C, indicating the decomposition reaction involving water and hydrocarbon molecules, resulting in a 6 % total mass loss. Despite the total binder components constituting only ~6 % in the coated NVP/C sheet, the TGA profile up to 550 °C reveals incomplete mass losses in the binder system, evident from residual masses observed in each binder component (Fig. 3) i.e., rest mass 1.37 % SBR (40 % from total), 0.36 % CMC (39 % from total) and 0.46 % PAA (20 % from total). This suggests that some of the conductive carbon (carbon black) within the slurry actively participates in reactions with the binder system. On the contrary, the HC-coated sheet in Fig. 4b exhibits an earlier onset of mass loss at 150 °C, attributed to the release of water molecules. This occurrence indicates the thermal decomposition of the binder, ruling out water absorption as a cause, given that the electrodes were thoroughly dried at 60 °C for 24 h in the glovebox under 10^{-3} bar. The released oxygen (although intensity is low to detect) combines with protons, resulting in the formation of H_2O, also seen in PAA binder (Fig. 3c). To ensure the reliability of the results, the measurements were duplicated to assess the homogeneity of the coated sheet. The difference in mass change of pristine electrode is ±0.04 % and at SOC100 % is ±0.15 % (Fig. S1). Subsequently, a complex thermal decomposition of the binder and its reaction with carbon occur, leading to the substantial evolution of CO/CO_2. Despite the total binder content being 5.6 % and 1.4 % carbon black, a total mass loss of ~8.5 % is observed. This implies that some of the HC also actively participates in the reaction.

After disassembling the coin cells at various charge states, the electrodes were purified by washing with DMC and thoroughly dried under vacuum of 10^{-3} bar for 24 h at 60 °C. Thereafter, the thermal stability of the corresponding electrodes was studied in a manner similar to that of pristine electrode materials. A noticeable early onset of mass loss at 100 °C was observed in all charge states (Fig. 5). Even at a state of charge (SOC) of 0 %, the same trend was observed for all NVP/C electrode sheets, revealing the reactivity of the formed cathode electrolyte interphase (CEI) with the binder system. This is also observed with NVP material with PVDF binder which is most probably a result of a surface reaction with PVDF or cathode–electrolyte interphase (CEI) components [25]. The binder components, which contain a hydroxyl group (OH), react with protons, forming water molecules at this temperature. This reaction is evident even at SOC 0 %, indicating the involvement of CEI in accelerating reactions that lead to the evolution of hydrocarbon and CO/CO_2 gases (Fig. 5). The mass spectrum of SOC 100 % was combined in Fig. 5, as the state-of-charge-dependent mass loss trend was consistent with the other states. This weird effect was not observed in the pristine electrode, as shown in Fig. 4a. The intensity of the reaction tends to decrease beyond 250 °C, contributing to a small amount of mass loss (i.e., 3 %) after 250 °C. Fig. 5 illustrates that mass loss increases with the state of charge, consistent with the expected lower thermal stability of the pristine cathode material due to the higher number of vacancies in the crystal lattice [26,27]. A similar trend with various states of charge was also reported for Prussian blue analogues material for sodium-ion batteries [28]. It should be noted, however, that in the X-ray analysis, when the charged NVP/C electrode was heated at an intermediate temperature range, the sodiated phase was observed [29]. Observed phases were close to the intermediate composition of $Na_2V_2(PO_4)_3$, which indicates an incomplete phase transition. An increase in vacancies in the lattice causes a decrease in thermal stability because it disrupts the crystal structure, enhances diffusion processes, weakens mechanical properties, potentially undergoes phase transformations due to redox reaction, and alters thermal expansion/contraction behaviour.

In the case of HC, a completely opposite trend was observed. Separately TGA-MS measurements of each harvested HC are given in supplementary information (Fig. S2). The thermal stability of the HC electrode demonstrated an increase with the states of charge, indicating that the polymeric binder formed complexes with sodium ions, thereby stabilizing the harvested HC electrode until 550 °C (Fig. 6a). To investigate whether this effect was solely attributed to the water-based binder system, a slurry with an organic solvent-based PVDF binder (with the same binder contents e.g., carbon black 1.40 wt.%, PVDF 5.60 wt.%) was additionally prepared, and an HC electrode was fabricated on copper (Cu) current collector. The pristine PVDF-HC electrode shows first mass loss onset temperature of 120 °C (evolved H_2O molecules) followed by second mass loss beyond 400 °C which is typical for PVDF binder (Fig. S3). A systematic thermal stability of the PVDF-based HC at equivalent states of charge was examined. Surprisingly, the same trend was identified; the PVDF binder-based HC also exhibited an increase in thermal stability with rising state of charge (Fig. 6b). The electrodes at different SOCs start to decompose at 300 °C despite of the thermal stability of pristine PVDF binder is beyond 400 °C [30,31]. The total mass loss was found to be dependent on the mass gain after charging in the HC electrode (Fig. 6c). In the case of the water-based binder, the mass gain did not show remarkable changes, leading to no significant difference in states of charge at 60 %, 80 %, and 100 %. In contrast, the PVDF-based HC displayed a linear increase in mass gain, contributing to the overall mass loss at states of charge of 60 %, 80 %, and 100 %. An unclear mass gain was observed at 40 % state of charge for the water-based HC, yielding to the higher mass loss during the heating of this electrode. The XRD investigation which can also be found in the supplement (Fig. S4) shows the formation of some sodium carbides after formation step, which agrees well with literature XRD results [32,33]. Comparison with works of literature indicate the presence of sodium carbide, attributed by main peaks at 2 theta (Θ) values of approximately 22°, 26°, 30°, 35°, 37°, 39°, 44°, and 46° These peaks are attributed to sodium carbide. Additionally, the XRD pattern exhibits sharp, prominent peaks at 43° and 51°, corresponding to pure copper. since the HC-PVDF slurry was coated on a copper foil substrate.

According to Fig. S5 (supplementary), the pure electrolyte exhibits two exothermic reactions at peak temperatures of 253 °C and 274 °C which is in good agreement with literature of $NaClO_4$ in carbonate solvents [34]. At temperatures above 250 °C, the electrolytes decomposed thermally, causing exothermic heat and it can be deduced that Na-salt electrolytes are more thermally stable than Li-salt electrolytes [34]. The released heat for these reactions is measured and calculated by integrating the corresponding peak area giving 4.5 J/g and 720 J/g respectively, which is due to the thermal decomposition [35,36]. Pure sodium perchlorate ($NaClO_4$) is known to undergo thermal decomposition under elevated temperature beyond 450 °C [37–39] and decomposition results in the formation of sodium salt (e.g. NaCl) and oxygen gas (O_2) [40]. Gas chromatography-mass spectrometry (GC–MS)

Table 2
Evolved gases during binder thermal decomposition.

Mass number	Evolved gases
2	H_2
18	H_2O
28	N_2, C_2H_4, CO
40	C_3H_4, Ar
44	CO_2, C_3H_6
46	C_3H_8

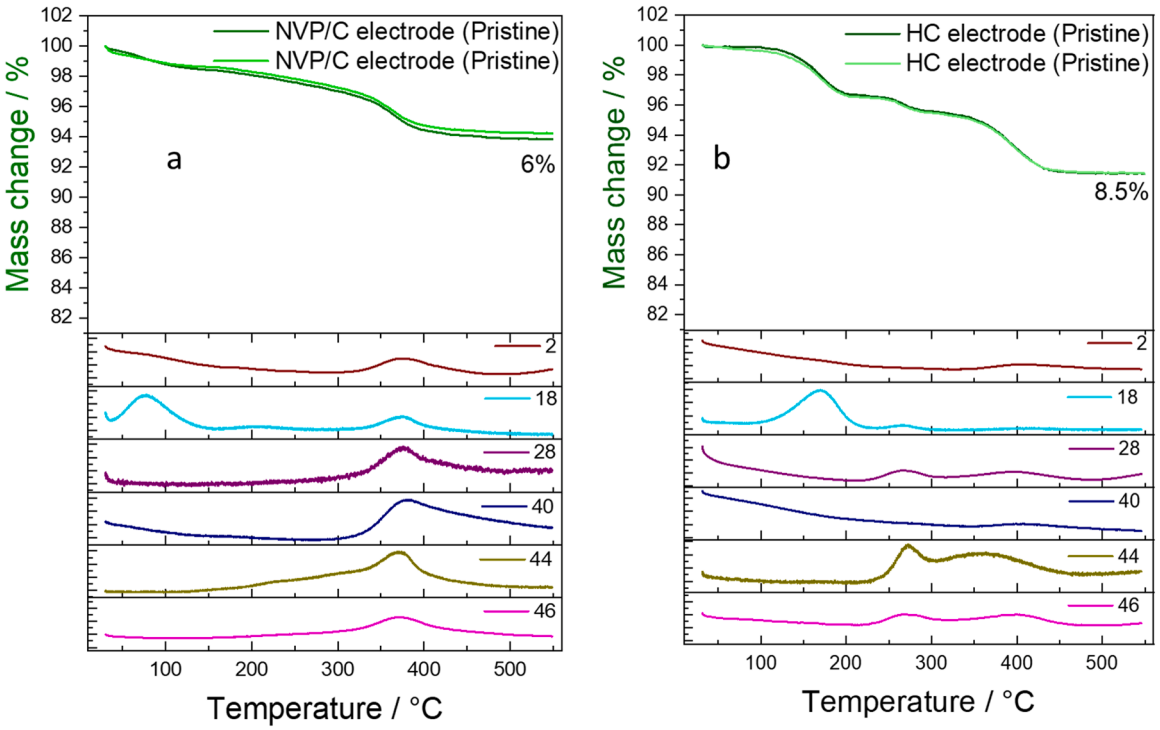

Fig. 4. Thermal stability of coated electrode sheet (a) NVP/C, (b) HC.

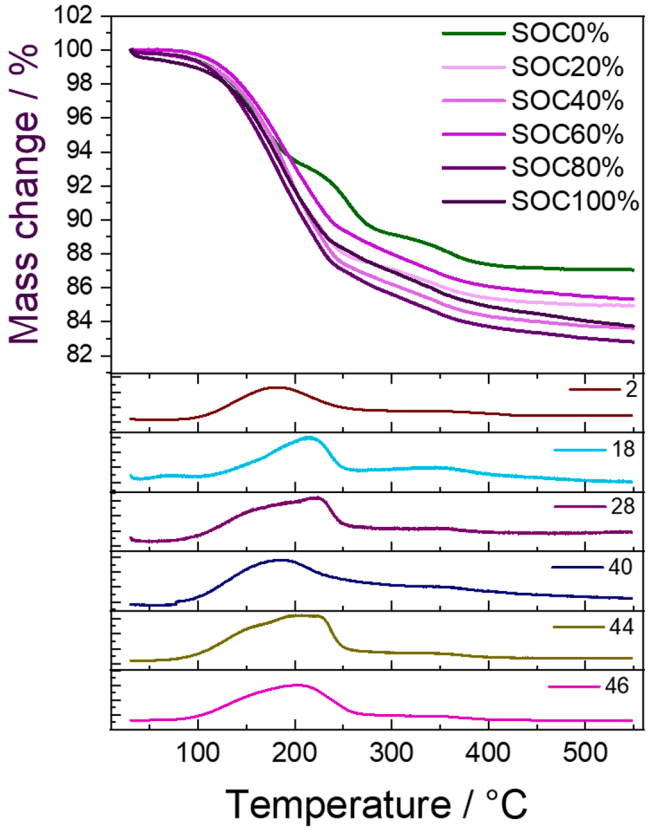

Fig. 5. Thermal stability data of NVP/C at different states of charge: mass loss comparison with mass spectrum at a SOC of 100 %.

analysis confirmed the liquid composition of the electrolyte (Fig. S6). The vaporization temperatures of each solvent are reported as EC 244 °C, DMC 91 °C, EMC 107 °C [41], which further helps in interpretation of the reactions. The initial decomposition temperatures for the individual solvents are reported as follows: DMC exhibited a decomposition temperature of 247 °C and EMC at 264 °C [42] . Botte et al. [43] revealed that EC undergoes decomposition at 263 °C, producing gases such as CO_2, O_2, and H_2. Additionally, EMC undergoes thermal decomposition in the presence of O_2, occurring between 220 °C and 235 °C and generating mainly CO_2 including the traces of O_2 and H_2 gases.

When the electrode materials are heated in conjunction with the electrolyte, the heat released is found to be highly dependent on the ratio of the material to the electrolyte. To uphold experimental precision, the use of fresh electrolyte was avoided and the electrodes with electrolyte were employed for subsequent experiments after disassembling. This approach, to include the mass of the existing electrolyte, was chosen to maintain consistency and ensure that the system remained unchanged. It is noteworthy that the fresh electrolyte incorporates the Solid Electrolyte Interphase (SEI) stabilizing additives (e.g., FEC in our case), which is consumed during the coin cell formation process. Utilizing fresh electrolyte in experiments could potentially alter the reaction mechanism due to the presence of such additive. Thus, such an approach is considered as non-realistic and might compromise the reliability and relevance of the experimental findings.

To examine the thermal reactivity impact of electrolytes on pristine electrodes, namely NVP/C and HC with CMC-SBR binder system, a calorimetric investigation was conducted both with and without electrolyte. The calorimetric curves (refer to Fig. S7) indicate a negligible effect on HC, while demonstrating a notable thermal impact on NVP/C materials above 200 °C.The 3D calorimetric analysis of charged NVP/C electrodes at various state of charges reveals crucial insights, as depicted in Fig. 7. Notably, NVP/C initiates decomposition at 160 °C, releasing a noteworthy amount of heat of 300 J/g to 400 J/g upon heating. This indicates the thermodynamic instability of NVP/C at low sodium content. Concurrently, Fig. 5 illustrates an obvious weight loss starting at 150 °C, accompanied by the presence of H_2O and O_2 molecules in the residual gas, indicative of a decomposition reaction. The ensuing broad

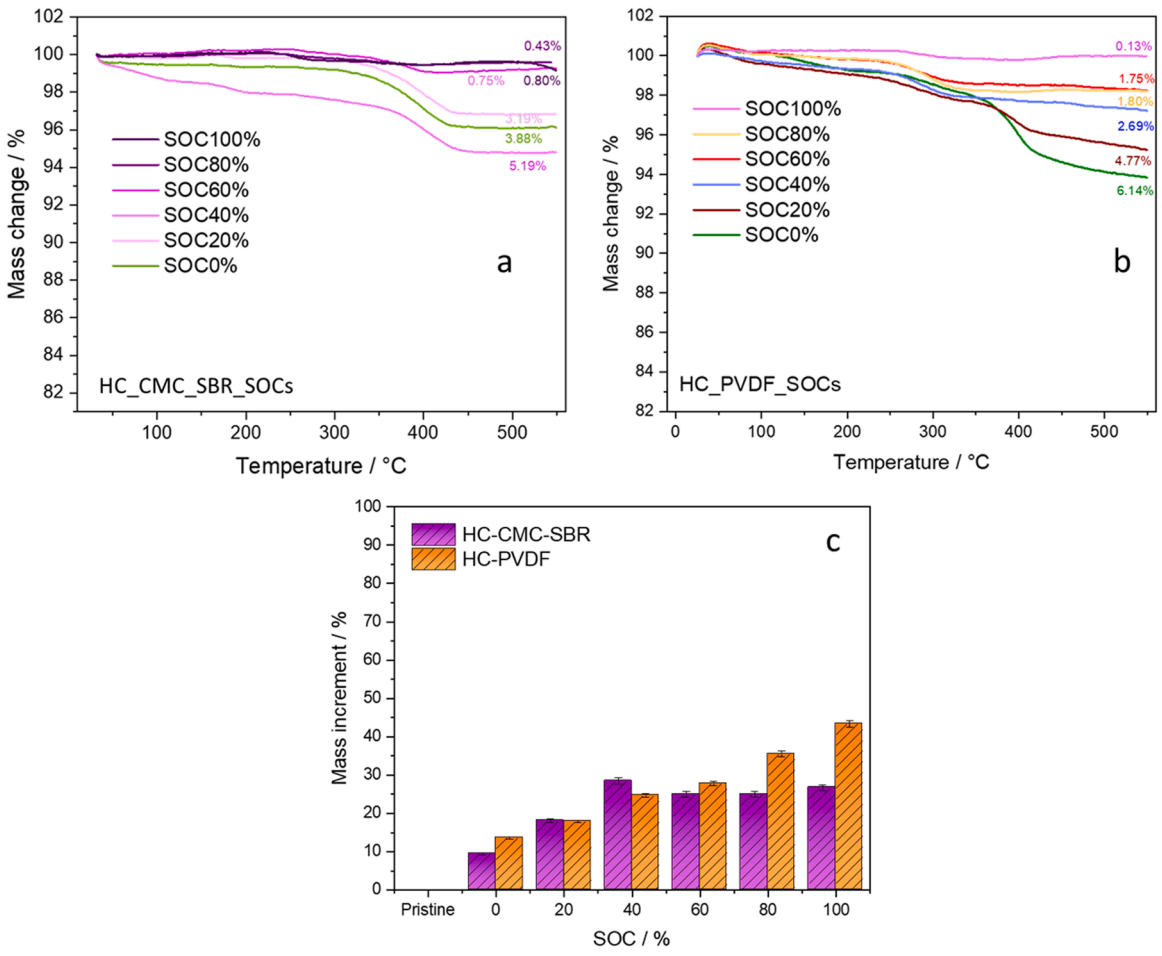

Fig. 6. Thermal stability data of harvested HC at different states of charge (a) HC with CMC-SBR binder, (b) HC with PVDF binder, (c) mass increment in both harvested-HC binder systems after cell disassembling and drying.

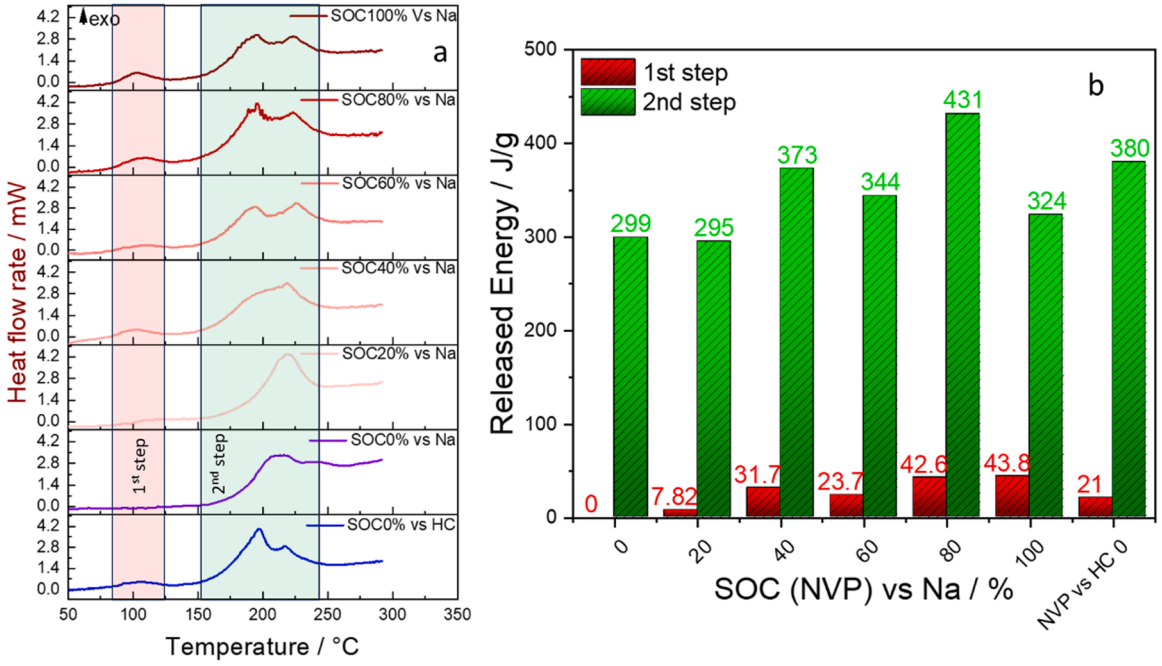

Fig. 7. Heat generation of NVP/C electrode with electrolyte at different state of charge vs Na/Na^{+} measured with C80 3D Tian-Calvet calorimeter: (a) comparison of heat flow rate vs. temperature curves (b) corresponding calculated released energy.

CO_2 peak results from the reaction between hierarchically structured carbon with NVP [44,45] and the released oxygen atoms. Moreover, when NVP/C is subjected to electrolyte-induced heating, an exothermic peak commences at approximately 150 °C (Fig. 7a). Remarkably, the released heat surpasses 300 J/g, implying combustion reactions with the organic solvent. Thus, we can conclude that when NVP/C is fully charged, it starts to decompose at ~200 °C with a significant amount of oxidative gases i.e., CO_2 (Fig. 5) and heat released which poses a potential safety hazard. Analysis of the calorimetric graph (Fig. 7a) reveals the relative stability of NVP/C below 160 °C. However, an additional state-of-charge-dependent exothermic reaction emerges between 100 °C and 120 °C, releasing ~10–50 J/g of heat, as illustrated in Fig. 7a and 7b as "step 1." Notably, this step 1 is absent at SOC0 %. Furthermore, in the first formation step (NVP/C against HC), some of the sodium content from NVP/C is consumed. Since NVP/C vs. HC is imbalanced capacity wise (Fig. S8) it shows similar values close to SOC40 % (~35 % irreversible capacity on HC during cell formation) as well as an exothermic reaction (step 1), releasing 21 J/g heat. This exothermic reaction is attributed to the reaction between the NVP/C-CEI and the solvent. Importantly, considering that the solvent does not decompose within this temperature range, the released heat is conclusively linked to the interaction between NVP/C-CEI and the solvent. More reactive CEI components can be formed due to the high charge potential that approaches the stability limit of carbonate electrolytes for sodium-ion batteries [25]. Accelerating rate calorimetry (ARC) studies by Xia et al., also showed the increase in reactivity of full de-intercalated Na_xCoO_2 with ethylene carbonate/diethyl carbonate (EC:DEC) solvent and $NaPF_6$/EC:DEC electrolyte [46]. However, intermediate de-intercalation steps are not considered in that investigation and only self-heating rates were measured based on the reaction reactivity. Zheng et al., have studied the heat generation of Prussian blue materials at low and high temperature regions and unveiled the generated heat increment with increase of de-sodiation, i.e. maximum heat released of 374 J/g at SOC100 % [28]. However, there are exothermic peaks between 125 °C −150 °C visible in which they did not explained. we can't conclude the specific trend of energy released (in 2nd step of NVP/C) depends on SOCs. The possible reason could be the cathode material reactivity with the electrolyte at this temperature is not dominant as the cathode material NVP/C is thermally stable at this temperature and seems less reactive even at low sodium contents. The reactivity of coated carbon/binders seems to be dominant which have the same amount in all electrodes at various SOCs. Nevertheless, the thermal stability of the cathode (NVP/C) also decreases at full charge state but at higher temperatures.

In the case of HC-harvested electrodes, the SOC0 % exhibits singular exothermal peaks within the temperature range of 150 °C-160 °C (Fig. 8a). These peaks are attributed to the thermal decomposition of the solid electrode interphase (SEI) [47], with a released energy of ~208 J/g. As temperatures ranged from 150 °C to 200 °C, sodiated HC and electrolytes produced the first mild exothermic heat. The peak was probably caused by the sodiated HC and electrolyte from SEI decomposition. It is also possible that the thermal degradation above 250 °C of excessive electrolyte contributed to the further exothermic heating of the mixtures [34] which was also seen in all-sodiated HC i.e. small exothermic curve upwards at 250 °C. Since the reaction is not accomplished until 300 °C, enthalpies of this exothermic reaction could not be calculated. In contrast, the HC formatted against NVP (as illustrated in Fig. S7 for the full cell) demonstrates smaller exothermic peaks compared to SOC0 % vs Na, indicating a generated heat of ~100 J/g. This reduction in heat is attributed to the incomplete formation of SEI when there is an imbalance in the full cell configuration. As the state of charge (SOC) increases, a second set of peaks emerges between 80 °C to 100 °C. The intensity of the first step (step 1) peak increases proportionally with the rise in SOCs from 60 % to 100 %. The second peaks (step 2) correspond to the SEI, and their intensities also exhibit an upward trend with increasing SOCs. The calculated energy for each respective peak is presented in Fig. 8b. Notably, the HC-harvested electrode displays a clear trend of incremental released energies for both steps, indicating an overall increase in heat release. At higher SOC levels, there is a decrease in the onset temperature and a significant increase in the self-heating rate, which was also reported for lithium-ion batteries [27]. These observations highlight the importance of considering the impact of SOCs on thermal behaviour, with implications for the design and performance of sodium-ion batteries. As far as battery safety is concerned, the heat generated by reactions between charged anodes and electrolytes is the most crucial factor which is proved in current studies in terms of exothermic heat.

The mass of electrodes and electrolyte, as listed in Table S1 in the

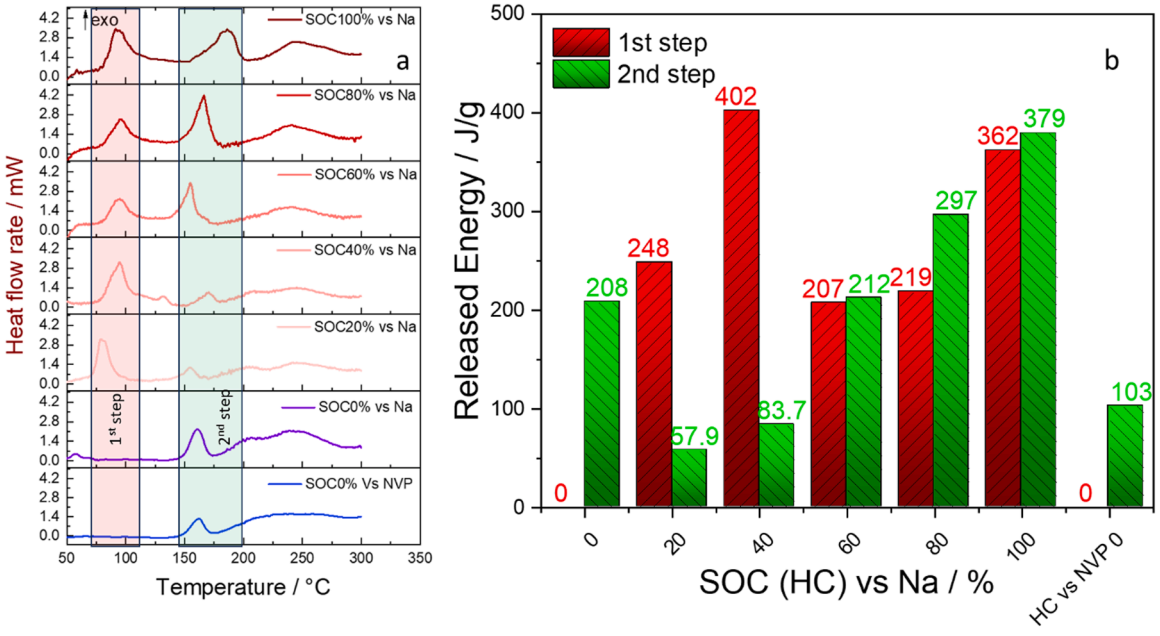

Fig. 8. Heat generation of HC electrode with electrolyte at different state of charge vs Na/Na^+: (a) comparison of heat flow rate vs. temperature curves (b) corresponding calculated released energy.

supporting information, reflects the harvested electrodes used after opening the coin cells. It is noteworthy that no additional electrolytes were subsequently introduced. Therefore, under these conditions it is hard to determine the exact amount of electrolyte in the respective electrodes.

4. Conclusion and outlook

Using a 3D Tian-Calvet calorimeter in the temperature range of 25 °C to 300 °C, NVP/C and HC electrodes for Na-ion batteries were evaluated for safety risk at different state of charge by analysing the generated heat. In addition the thermal stability of these materials was investigated at different state of charge by TGA-MS. It was revealed that the exothermic decomposition of the electrolyte (1 M $NaClO_4$ in EC:DMC: EMC = 1:1:1 + 2 wt.% FEC) between 270 °C and 280 °C can obscure the thermal signals from the materials. Consequently, it is crucial to limit the amount of electrolyte in such experiments. NVP/C exhibits the lowest stability, decomposing at 200 °C and releasing approximately 800 J/g heat. Additionally, NVP/C reacts with the electrolyte between 200 °C and 300 °C, releasing 400 J/g heat, although it does not exhibit the O_2 evolution issue observed typically in layered oxide materials. HC initiates decomposition at 100 °C, releasing ~750 J/g heat. Consequently, the thermal stability of charged NVP/C materials follows a decreasing order with increasing states of charge (SOCs). Notably, sodiated HC electrode materials remain stable in the presence of higher sodium contents and show increase in enthalpies with increase in states of charge. In summary, our study provides new insights into the thermal behaviour of Na-ion battery cathode and anode materials, highlighting the importance of considering binder systems and electrolyte limitations in such investigations.

The findings from this investigation will be incorporated into the prominent cell level formats such as sodium pouch and 18,650 cylindrical cells. Moreover, the state-of-charge-dependent thermal runaway events shall be identified. The self-heating rates corresponding to different SOCs will elucidate the intensities of self-triggered exothermic reactions.

Data availability statement

The raw data corresponding to the relevant measurements is openly accessible on Zenodo through the following DOI: 10.5281/zenodo.10617681

Declaration of competing interest

The authors declare the following financial interests/personal relationships which may be considered as potential competing interests:

Ijaz Ul Mohsin reports financial support was provided by German Research Foundation. Carlos Ziebert reports financial support was provided by German Research Foundation. If there are other authors, they declare that they have no known competing financial interests or personal relationships that could have appeared to influence the work reported in this paper.

Acknowledgments

The authors gratefully acknowledge Dr. Klaus Seemann for his assistance with the XRD analysis and Mr. Xuebin Wu, Dr. Pirmin Stüble and Dr. Ulrike Kaufmann for providing water-based binder system / coated NVP/C electrode sheets. We would like to thank Julian Klemens, Dr.-Ing. Philip Scharfer and Prof. Dr.-Ing. Wilhelm Schabel from Thin Film Technology at KIT for coating and drying high quality HC electrodes in the TFT Coating and Printing Lab within the scope of the joint research in the DFG Cluster of Excellence POLiS. This work contributes to the research performed at CELEST (Center for Electrochemical Energy Storage Ulm-Karlsruhe) and was funded by the German Research Foundation (DFG) under Project ID 390874152 (POLiS Cluster of Excellence, EXC 2154).

Supplementary materials

Supplementary material associated with this article can be found, in the online version, at doi:10.1016/j.electacta.2024.144197.

References

[1] J.J. Braconnier, et al., Comportement electrochimique des phases NaxCoO2, Mater. Res. Bull. 15 (12) (1980) 1797–1804.
[2] P. Gotcu, et al., Thermal behaviour of LixMeO2 (Me = Co or Ni + Mn + Co) cathode materials, Phys. Chem. Chem. Phys. 19 (19) (2017) 11920–11930.
[3] P. Gotcu, H.J. Seifert, Thermophysical properties of LiCoO2–LiMn2O4 blended electrode materials for Li-ion batteries, Phys. Chem. Chem. Phys. 18 (15) (2016) 10550–10562.
[4] R.E. Williford, V.V. Viswanathan, J.G. Zhang, Effects of entropy changes in anodes and cathodes on the thermal behavior of lithium ion batteries, J. Power. Sources 189 (1) (2009) 101–107.
[5] S.C. Chen, C.C. Wan, Y.Y. Wang, Thermal analysis of lithium-ion batteries, J. Power. Sources 140 (1) (2005) 111–124.
[6] G. Hautier, et al., Phosphates as lithium-ion battery cathodes: an evaluation based on high-throughput ab initio calculations, Chem. Mater. 23 (15) (2011) 3495–3508.
[7] I.U. Mohsin, et al., Thermophysical characterization of a layered P2 type structure Na0.53MnO2 cathode material for sodium ion batteries, Batteries 7 (2021), https://doi.org/10.3390/batteries7010016. . (Basel).
[8] I.U. Mohsin, et al., Enabling the electrochemical performance of maricite-$NaMnPO_4$and maricite-$NaFePO_4$cathode materials in sodium-ion batteries, Int. J. Electrochem. 2023 (2023) 6054452.
[9] S.Y. Lim, et al., Electrochemical and thermal properties of NASICON structured Na3V2(PO4)3 as a sodium rechargeable battery cathode: a combined experimental and theoretical study, J. Electrochem. Soc. 159 (9) (2012) A1393.
[10] T. Jin, et al., Polyanion-type cathode materials for sodium-ion batteries, Chem. Soc. Rev. 49 (8) (2020) 2342–2377.
[11] J. Zhao, et al., Electrochemical and Thermal Properties of α-NaFeO2 Cathode for Na-Ion Batteries, J. Electrochem. Soc. 160 (5) (2013) A3077.
[12] W. Kobayashi, et al., Thermal expansion in layered NaxMO2, Sci. Rep. 8 (1) (2018) 3988.
[13] S.M. Bak, et al., Thermal stability studies in charged layered sodium transition metal oxide cathode materials for Na-ion batteries, ECS Meet. Abstr. MA2015-02 (4) (2015) 338.
[14] C.Y. Jiang, et al., Thermal cycling behavior of nanostructured and conventional yttria-stabilized zirconia thermal barrier coatings via air plasma spray, Rare Met. 42 (11) (2023) 3859–3869.
[15] K. Yan, J. He, H.B. Guo, High-temperature oxidation behaviour of minor Hf-doped β-NiAl single crystals in dry and humid atmospheres, Rare Met. 42 (8) (2023) 2767–2773.
[16] M. Guilmard, L. Croguennec, C. Delmas, Thermal stability of lithium nickel oxide derivatives. Part II: LixNi0.70Co0.15Al0.15O2 and LixNi0.90Mn0.10O2 (x = 0.50 and 0.30). Comparison with LixNi1.02O2 and LixNi0.89Al0.16O2, Chem. Mater. 15 (23) (2003) 4484–4493.
[17] I. Belharouak, et al., Safety characteristics of Li(Ni0.8Co0.15Al0.05)O2 and Li(Ni1/3Co1/3Mn1/3)O2, Electrochem. Commun. 8 (2) (2006) 329–335.
[18] Z. Li, et al., Stability and rate capability of al substituted lithium-rich high-manganese content oxide materials for Li-ion batteries, J. Electrochem. Soc. 159 (2) (2011) A116.
[19] V.L. Chevrier, et al., Isothermal calorimetry evaluation of metallurgical silicon as a negative electrode material for Li-ion batteries, J. Electrochem. Soc. 168 (3) (2021) 030504.
[20] M.S. Whittingham, Ultimate limits to intercalation reactions for lithium batteries, Chem. Rev. 114 (23) (2014) 11414–11443.
[21] J. Klemens, et al., Process and drying behavior toward higher drying rates of hard carbon anodes for sodium-ion batteries with different particle sizes: an experimental study in comparison to graphite for lithium-ion-batteries, Energy Technol. 11 (8) (2023) 2300338.
[22] J. Klemens, et al., Challenges and opportunities for large-scale electrode processing for sodium-ion and lithium-ion battery, Batter. Supercaps 6 (11) (2023) e202300291.
[23] I.U. Mohsin, et al., Heat generation and degradation mechanisms studied on Na3V2(PO4)3/C positive electrode material in full pouch /coin cell assembly, J. Power Sources 545 (2022) 231901.
[24] E. Gibertini, et al., Algae-derived hard carbon anodes for Na-ion batteries, J. Appl. Electrochem. 51 (12) (2021) 1665–1673.
[25] R.R. Samigullin, et al., Thermal stability of NASICON-type Na3V2(PO4)3 and Na4VMn(PO4)3 as cathode materials for sodium-ion batteries, Energies 16 (7) (2023) 3051. . (Basel).
[26] Y. Huang, et al., Thermal stability and reactivity of cathode materials for Li-ion batteries, ACS Appl. Mater. Interfaces 8 (11) (2016) 7013–7021.
[27] A. Kvasha, et al., A comparative study of thermal runaway of commercial lithium ion cells, Energy 159 (2018) 547–557.

[28] Z. Li, et al., Revealing the thermal safety of prussian blue cathode for safer nonaqueous batteries, Adv. Energy Mater. 11 (42) (2021) 2101764.
[29] S. Park, et al., Crystal structure of Na2V2(PO4)3, an intriguing phase spotted in the Na3V2(PO4)3–Na1V2(PO4)3 system, Chem. Mater. 34 (1) (2022) 451–462.
[30] Jesus de, A.J. Silva, et al., Kinetics of thermal degradation and lifetime study of poly(vinylidene fluoride) (PVDF) subjected to bioethanol fuel accelerated aging, Heliyon 6 (7) (2020) e04573.
[31] J. Ma, R.I. Haque, R.M. Larsen, Crystallization and mechanical properties of functionalized single-walled carbon nanotubes/polyvinylidene fluoride composites, J. Reinf. Plast. Compos. 31 (21) (2012) 1417–1425.
[32] M.S. Swapna, S. Sankararaman, Organometallic sodium carbide for heat transfer applications: a thermal lens study, Int. J. Thermophys. 41 (7) (2020) 93.
[33] M.S. Swapna, et al., Natural precursor based hydrothermal synthesis of sodium carbide for reactor applications, Mater. Res. Express. 4 (12) (2017) 125602.
[34] J. Zhao, et al., Electrochemical and thermal properties of hard carbon-type anodes for Na-ion batteries, J. Power Sources 244 (2013) 752–757.
[35] H. Hijazi, P. Desai, S. Mariyappan, Non-Aqueous Electrolytes for Sodium-Ion Batteries: challenges and Prospects Towards Commercialization, Batter. Supercaps 4 (6) (2021) 881–896.
[36] A. Hofmann, et al., electrolyte mixtures based on ethylene carbonate and dimethyl sulfone for Li-ion batteries with improved safety characteristics, ChemSusChem 8 (11) (2015) 1892–1900.
[37] G.G. Eshetu, et al., Electrolytes and interphases in sodium-based rechargeable batteries: recent advances and perspectives, Adv. Energy Mater. 10 (20) (2020) 2000093.
[38] P. Deng, H. Ren, Q. Jiao, Enhanced thermal decomposition performance of sodium perchlorate by molecular assembly strategy, Ionics 26 (2) (2020) 1039–1044. . (Kiel).
[39] X. He, et al., Comparison study of electrochemical and thermal stability of Na3V2 (PO4)3 in different electrolytes under room and elevated temperature, Int. J. Energy Res. 46 (15) (2022) 23173–23194.
[40] D.J. Devlin, P.J. Herley, Thermal decomposition and dehydration of sodium perchlorate monohydrate, React. Solids 3 (1) (1987) 75–84.
[41] J. Lamb, et al., Studies on the thermal breakdown of common li-ion battery electrolyte components, J. Electrochem. Soc. 162 (10) (2015) A2131.
[42] Y. Fernandes, A. Bry, S. de Persis, Thermal degradation analyses of carbonate solvents used in Li-ion batteries, J. Power Sources 414 (2019) 250–261.
[43] G.G. Botte, T.J. Bauer, MRSST a new method to evaluate thermal stability of electrolytes for lithium ion batteries, J. Power Sources 119-121 (2003) 815–820.
[44] T. Akçay, et al., Na3V2(PO4)3—A highly promising anode and cathode material for sodium-ion batteries, ACS Appl. Energy Mater. 4 (11) (2021) 12688–12695.
[45] W. Bauer, et al., Using hierarchically structured, nanoporous particles as building blocks for NCM111 cathodes, Nanomaterials 14 (2024), https://doi.org/10.3390/nano14020134.
[46] X. Xia, J.R. Dahn, A study of the reactivity of De-Intercalated P2-NaxCoO2 with non-aqueous solvent and electrolyte by accelerating rate calorimetry, J. Electrochem. Soc. 159 (5) (2012) A647.
[47] I.U. Mohsin, et al., Comprehensive electrochemical, calorimetric heat generation and safety analysis of Na0.53MnO2 cathode material in coin cells, J. Electrochem. Soc. 168 (5) (2021) 050544.